B.Sc. (Hons) Physics Project

Thesis

Samuel Moore
School of Physics, University of Western Australia
April 2012

Characterisation of Nanostructured Thin Films

Keywords: surface plasmons, nanostructures, spectroscopy, metallic-blacks
Supervisers: W/Prof. James Williams (UWA), Prof. Sergey Samarin (UWA)

Contents

Acknowledgements

I am extremely grateful for the support offered to me by many individuals during this project. There aren't many synonyms for "Thanks", so I'm afraid this section may be a little repetitive.

Thanks to my supervisors Prof Sergey Samarin and W/Prof Jim Williams for envisioning the project, and their invaluable support throughout the year. I would also like to thank staff members at CAMSP for assisting with the supervision of this project. In particular I am extremely grateful for the help and advice given by Dr Paul Gualiardo during the construction and testing of the Total Current Spectroscopy experiment.

Thanks to Alexie ??? from CMCA for producing the SEM images which proved a invaluable aid for discussing the structure of the metallic-black films. Thanks to Nikita Kostylev for helping me learn the art of operating the ellipsometer. Thanks to both Prof Mikhail Kostylev and Jeremy Hughes for lending me some samples for ellipsometric analysis. I would also like to endorse the team at J.A Woolam, who provided replacement pins for the ellipsometer alignment detector at no charge after one of the original pins became mysteriously damaged.

Congratulations to Jeremy Hughes who successfully predicted that the emission current of the electron gun was varying periodically less than a quarter of the way through the first period. Condolences to Alexander Mazur, whose theory that the vacuum chamber contained a pulsar proved unfounded.

Thanks to all my family and friends for their support and for continuing to put up with my slow descent into madness during the last 12 months.

Finally, perhaps as a result of the aforementioned madness, I would also like to thank the various pieces of equipment and inanimate objects which have been crucial to the success of this project. This includes the ellipsometer, the ADC/DAC box, my laptop computer "Cerberus", and the two ammeters upon which I relied upon so heavily. Rest in peace Keithly 610B. Your death was not in vain.

1 Introduction

The report will be organised as follows; first we will discuss literature relating to surface science and nanostructured thin films in particular. We will then give an overview of the primary experimental techniques employed during this project, before presenting experimental results. Finally, we will discuss stuff.

2 Overview

In this section we provide an overview of theoretical and experimental literature related to the properties of nanostructured thin films. We also include a summary of the past research which focuses on metallic-black films.

2.1 Secondary Electron Emission

Secondary electron emission refers to the emission of electrons from a target surface caused by interactions with an incident electron, or more commonly a beam of electrons. Electrons from the incident beam are referred to as primary electons, whilst the term "secondary electron" applies to all electrons reflected or emitted from the surface under bombardment.

Figure 1 shows the general shape of an energy distribution of secondary electrons. for a primary electron energy of E_p. The narrow peak centred at $E = E_p$ is due to elastically scattered electrons; the width of this peak is determined by the distribution of primary electron energies, as well as the resolution of the detector. The broad peak in the low energy part of the spectrum is due to inelastically scattered electrons.

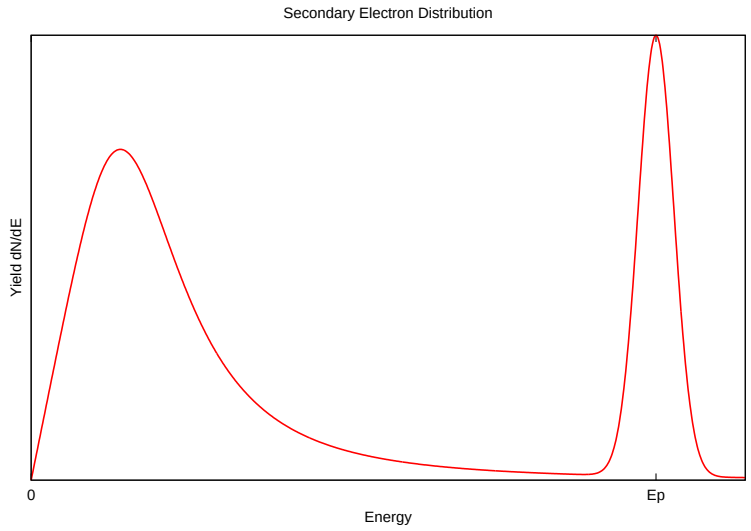

Figure 1: **Model of Secondary Electron Distribution**

Real secondary electron distributions also show fine structure imposed upon the inelastic part of simplified spectrum described above. This fine structure is characteristic of the electron spectra of the target surface. Near to the elastic peak, fine structure is caused by energy loss to interband transitions and plasma vibration excitation. The central part of the distribution contains fine structure due to Auger electron emission, and energy losses due to excitation of inner electrons. Fine structure at low energies is due to the structure of empty states of the solid.

2.2 Plasmons

A plasmon is a quasi-particle arising due to charge density oscillations in a solid.

2.3 Metallic-Black Films

So called metallic-black films are the result of deposition of metal elements at a relatively high pressure (of the order of 10^{-2} mbar). The films are named due to their high absorbance at visible wavelengths; they appear black to the naked eye. There is a remarkable contrast between such films and films deposited under low pressure (less than 10^{-6}mbar), which are typically highly reflective and brightly coloured.

This phenomenom has been known since the early 20th century, with the first papers on the subject published by Pfund in the 1930s [1], [2]. Pfund established the conditions for formation of metallic-blacks [1], and showed that the transmission spectrum of metallic black films is almost zero in visible wavelengths, but increases to a plateau in the far infrared [2]. More extensive research on the structural and optical properties of these films by Louis Harris and others during the 1940s and 1950s [3], [4], [5]. It has been established that metallic blacks may be prepared in either air or inert gases

Secondary Electron Microscope (SEM) images of Au deposited on Si at high and low pressures (in air) were produced at the Centre for Microscopy Characterisation and Analysis (CMCA), UWA. The film imaged on the left (high pressure) appears black at visible wavelengths, whilst the film on the right (low pressure) appears golden yellow.

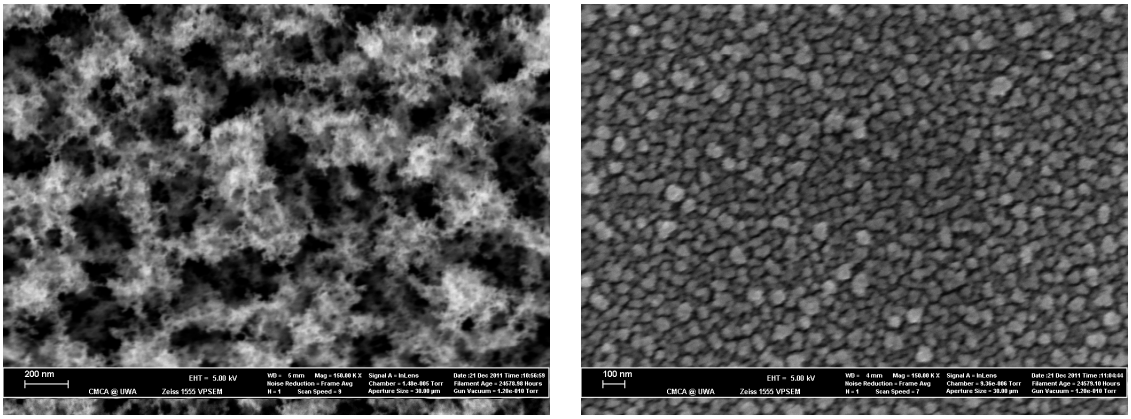

Figure 2: **SEM images of Au deposited on Si at 2×10^{-2}mbar (left) and 1×10^{-6}mbar.** Note that the scales are very similar for both images.

The structural difference between the two films is striking, and yet the exact mechanism behind the formation of the metallic-black film is not well understood. The most widely accepted explanation is that the evaporated metal particles reaching the target surface have insufficient energy to form a regular crystal lattice due to cooling through collisions with the atmosphere []. As of yet, there is no detailed theoretical description of this behaviour.

Harris et al. have produced experimental results of the transmission of metallic-black films from visible wavelengths to the far-infrared []. By modelling the film as a layer of metallic strands, acting as "condensors", Harris et al. arrived at an expression for the electron relaxation time of [element]-black [], leading to a a transmission spectrum in good agreement with experimental results.

Mckenzie has established that the presence of oxygen effects the optical and electrical properties of metallic-blacks [6].

Nanostructured metal films prepared at low pressure are often approximated by an isotropic layer of spherical blobs upon the substrate, or even as a uniform layer with an "effective" thickness []. As the right image in Figure 2.3 shows, this is a good representation of the structure of such a film. In contrast, the metallic-black film is highly non-uniform; as a result, detailed characterisation of the properties of such a film is difficult.

More recently, it was shown that Au-black coatings increased the efficiency of thin film solar cells []. In this study, a simulation approximating an Au-black film as a layer of semi-spherical structures showed plasmonic behaviour which lead to an increase in electric field behind the film.

Metallic-black films have proven useful in applications requiring efficient absorption of light, including the. Recently there has been interest in artificial "blackening" of metal surfaces in ways which simplify the characterisation of the surfaces for practical applications.

Sondergaard et al. have produced metallic-black surfaces capable of suporting surface plasmon modes [7]. These films exhibit similar optical properties to the previously considered "evaporated" metallic-black surfaces.

This project will employ Total Current Specroscopy, Ellipsometry and Optical Spectroscopy methods to investigate the difference between metallic films deposited at low pressure, and high pressure (metallic-blacks). The production and study of artificially blackened films is beyond the scope of this research.

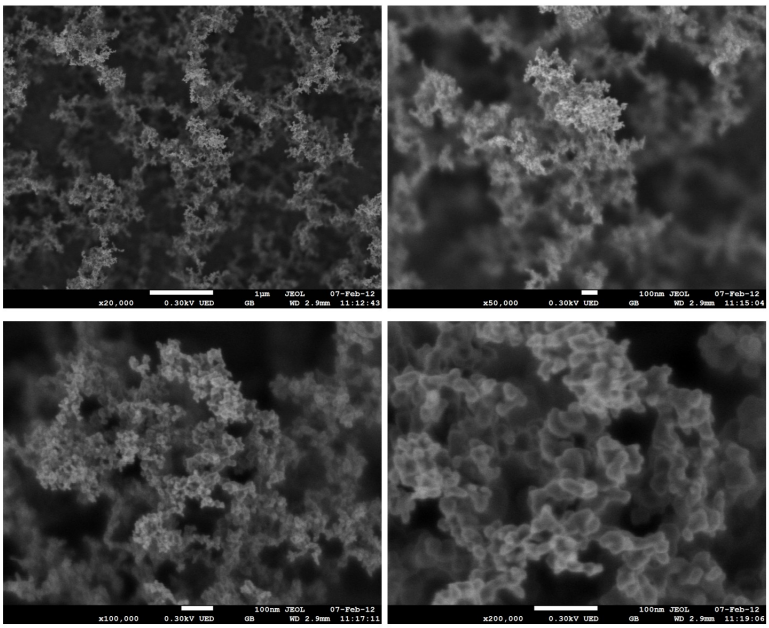

Figure 3: **Au-black film viewed at magnifications of x20000, x50000, x100000 and x200000** (top left, top right, bottom left, bottom right). The film appears non-isotropic, and possibly fractal like upon magnification. This structure has lead some reasearchers to refer to the deposited films as "smokes" [].

3 Experimental Techniques

3.1 Secondary Electron Spectroscopy

Secondary Electron Spectroscopy encompasses a large group of techniques which exploit secondary electron emission for studying the electron spectra of surfaces and solids. In these methods a beam of primary electrons is directed at a surface. The interactions between primary electrons and the surface give rise to an energy distribution of electrons elastically and inelastically scattered from the surface. Analysis of the distribution of the scattered "secondary" electrons gives information about the electron energy spectrum of the target surface.

Techniques of Secondary Electron Spectroscopy can be divided into two classes. Energy-resolved methods are based upon observation of the secondary electron distribution at a fixed primary electron energy. These methods aim to examine specific secondary emission processes which occur within a selected energy interval. The angular distribution of emitted electrons is often also recorded.

In contrast to Energy-resolved methods, Total Current (or Yield) methods measure the total current of secondary electrons as a function of primary electron energy. The focus of this project has been low energy Total Current Spectroscopy (TCS). While Total Current methods provide less detailed information about secondary emission processes within a solid, they are generally simpler to realise experimentally as they do not require energy analysers, and current measurement may be performed external to the vacuum chamber.

3.2 Total Current Spectroscopy

Figure **??** shows a simplified schematic for the Total Current Spectroscopy experiments conducted during this study. An electron gun is used to produce the beam of primary electrons. Electrons are emitted from a cathode held at negative potential relative to the target. These electrons are focused into a beam and accelerated onto the target through the electric field produced by a series of electrodes. A detector is used to measure the total current passing through the target.

A major advantage of Total Current Spectroscopy methods is the relative simplicity of the experimental setup. Because energy resolution of secondary electrons is not required, current measurement can be performed external to the vacuum chamber, using a conventional ammeter.

If the current incident upon the sample is I_{total}, and the current of secondary electrons scattered from the surface is I_r, then the transmitted current I_t is given by:

$$I_t = I_{\text{total}} - I_r$$

Generally I_{total} is assumed to be independent of initial energy E. This assumption is valid if the initial energy is small compared to the accelerating potential of the gun, and the distance of the sample from the gun is sufficiently large.

In this case, differentiating with respect to E:

$$\frac{dI_t}{dE} = -\frac{dI_r}{dE}$$

Figure 3.2 is a block diagram of the experimental setup including measurement and control systems external to the vacuum chamber. Note that the emission current ammeter is optional, and was used for testing purposes.

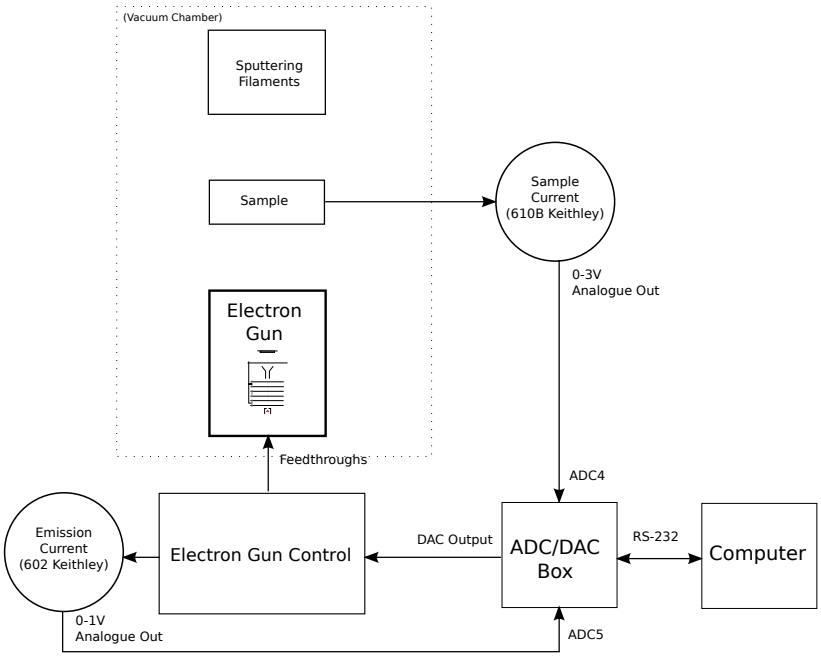

3.2.1 Electron Optics

The electron gun used for this experiment was repurposed from an old Cathode-Ray Oscilloscope (CRO). Figure **??** shows a simplified diagram of the electron gun, whilst Figure **??** shows a photograph of the gun.

The full circuit diagram for the electron gun control circuit is shown in Appendix A.

3.2.2 Automatic Data Acquisition

In order to collect data on the large number of planned samples for the study, some form of automation was required. The automated system needed to be able to set the initial energy by adjusting the potential of the cathode relative to the sample, and simultaneously record the total current through the sample.

The available power supplies at CAMSP featured analogue inputs for external control. This meant that a Digital to Analogue Convertor (DAC) card was needed to interface between the control computer and the power supply. In addition, the available instruments for current measurement produced analogue outputs. As a result, Analogue to Digital Convertors (ADCs) were required to automate the recording of total current.

Although an external DAC/ADC box was already available for these purposes, initial tests showed that the ADCs on the box did not function. The decision was made to design and construct a custom DAC/ADC box, rather than wait up to two months for a commercial box to arrive. The design of the custom DAC/ADC box is discussed in detail in Appendix B, and the software written for the on-board microprocessor and the controlling computer are presented in Appendix D.

3.3 Ellipsometry

Ellipsometry is an optical technique most commonly used to determine the thickness of multilayered thin films. Ellipsometry can also be used to determine the optical constants and properties of unknown materials.

Essentially, ellipsometry measures the change in polarisation of light reflected from a surface. This change in polarisation can be related to properties of the surface if knowledge of the surface is correctly applied. For a bulk sample, the change in polarisation can be directly related to the optical constants of the material.

A

3.3.1 Variable Angle Specroscopic Ellipsometry

A single ellipsometric measurement involves recording r_p and r_s at one angle and wavelength. The earliest ellipsometers were

A Variable Angle Spectroscopic Ellipsometer at CAMSP has been used to perform a variety of measurements on metallic thin films.,

The VASE

It is also possible to conduct reflection and transmission spectroscopy experiments using the VASE.

3.4 Vacuum Techniques and Sample Preparation

Both the TCS experiments and the deposition of films must be performed in a vacuum. For convenience and simplicity, a single vacuum chamber at CAMSP has been repurposed to perform both of these tasks. The chamber can be pumped by a molecular turbo pump, backed by a rotaray pump, to a base pressure of 2×10^{-8} mbar, or by the rotary pump alone to a base pressure of 1×10^{-3} mbar. The pressure is monitored using either a pirani or ion gauge (for pressures greater than and less than 10^{-3} mbar respectively).

Figure **??** shows a diagram of the vacuum chamber used both for the creation of nanostructured thin films and their study using TCS. A rotatable sample holder is positioned in the centre of the chamber. One flange of the chamber houses the electron gun used for TCS measurements, whilst the opposite flange contains feedthroughs on which tungsten filament evaporators are mounted. This setup allows for almost immediate study of evaporated films by simple rotation of the sample holder to face the gun.

The evaporators consist of a tungsten wire filament attached between two feedthroughs. A piece of a desired metal is folded over the apex of the tungsten wire. The metal can be heated by passing a current through the filament; near the metal's melting point it begins to evaporate. To clean the metal surface and ensure uniform evaporation, this procedure is first performed at low pressure (below 10^{-6} mbar) with no sample in the chamber, with the current increased until the metal piece begins to melt and forms a ball on the wire. Figure **??** shows an image of an evaporator that has been prepared for use.

This study focused primarily on depositing Au films on an Si substrate, at both high and low pressures. The substrates and sample holders were cleaned in an acetone bath immediately prior to insertion in the vacuum

chamber.

4 Experimental Results and Discussion

4.1 TCS Measurements

4.2 Ellipsometric Measurements

4.3 Transmission Spectra of Metal Films

Using the VASE and a commercial spectrometer (OceanOptics) in independent experiments, we obtained transmission spectra for metallic-black and some other metallic films.

5 Achievements

Appendix A - Electron Gun Control and Current Measurement Circuit

Figure **??** shows the complete electron gun control circuit. The circuit was designed and constructed as part of this project. The design is based upon examples found in [**?**] and [**?**].

Electron Optics

The electron gun has been recycled from a Cathode Ray Oscilloscope. Figure **??** shows a diagram and photograph of the gun. The gun contains a total of 9 electrodes; several electrodes are held at the same potential, as shown in the figure. As shown in figure **??**, the electrode potentials are referenced to the cathode, not signal ground. Because of the relatively large distance between the gun and sample (held at ground), this ensures that changes in initial energy do not significantly effect the focusing properties of the gun.

The optimum potentials of the gun electrodes were determined manually by focusing the gun on an Au film (deposited on Si). I-V curves obtained by measuring current through the sample as a function of initial energy were obtained. The electrode potentials were systematically altered to ensure the curves were as close as possible to the ideal model.

Model of I-V curves

The current detected through the sample is due to electrons which have sufficient energy to overcome the potential barrier between the surface and vacuum, entering the conduction band

The filament is surrounded by a conducting cylindrical electrode commonly called the "Venault". The potential of the venault has little effect on the focusing properties of the gun, but is largely responsible for determining the current leaving the gun. Figure **??** shows I-V curves for several venault settings, including the optimum setting.

Einzel Lens

Appendix B - DAC/ADC Box - Hardware

Overview

In order to automate TCS experiments, both Digital to Analogue and Analogue to Digital Convertors were required (DAC and ADC). To provide these, a custom DAC/ADC Box was designed and constructed. The box can be controlled by any conventional computer with available RS-232 serial communication (COM) ports. Most modern computers no longer feature COM ports; a commercially available convertor can be used to interface between the box's RS-232 output and a standard Universal Serial Bus (USB) port.

The key components of the DAC/ADC box hardware include:

- Microprocessor (AVR Butterfly ATMega169)
- Four Analogue to Digital Converter (ADC) inputs
- Single Digital to Analogue Converter (DAC) output (Microchip MCP4922)
- Analogue electronics for amplification at ADC inputs and DAC outputs
- Seperate power supply circuitry for Digital and Analogue electronics
- RS-232 communications for control by a conventional PC or laptop

Microprocessor

The DAC/ADC box has been based upon Atmel's AVR Butterfly; an inexpensive and simple demonstration board for the ATMega169 16 Bit microprocessor. The features of the AVR Butterfly include easily accessible ports for Analogue to Digital Convertor (ADC) inputs and digital input/output, an onboard Universal Asynchronous Reciever/Transmitter (USART) for RS-232 serial communications, and a 6 character Liquid Crystal Display (LCD). The AVR Butterfly can be programmed using a conventional computer over the USART using a RS-232 COM port. For modern computers (which do not usually posess COM ports), a RS-232 to USB converter may be used.

Figure 4 is a labelled photograph of the AVR Butterfly showing the use of the available ports for this project.

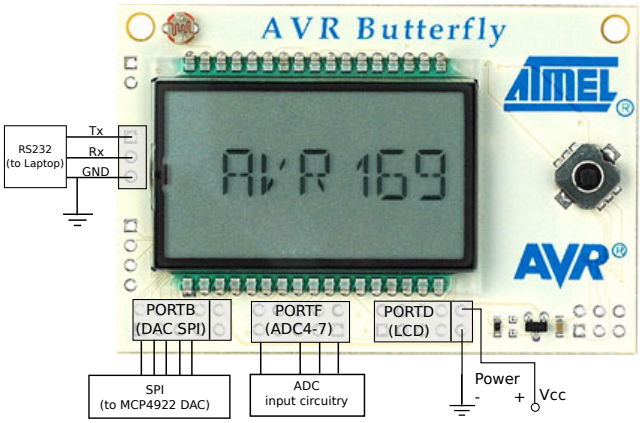

Figure 4: AVR Butterfly

Unless otherwise stated, all voltage differences are specified relative to the power supply ground of the AVR Butterfly.

ADC Inputs

The AVR Butterfly offers easy access to four of the ATMega169's ADCs through PORTF. Each ADC is capable of measuring voltages of $0 < V_{\text{adc}} < V_{cc}$ with 10 Bit resolution. For measuring voltages outside this range, some circuitry is required between the input voltage and the ADC input. In addition, it is desirable to provide the ADC with some form of input protection against accidental overloading. Figure 5 shows the input circuit which was used for three of the four available ADCs.

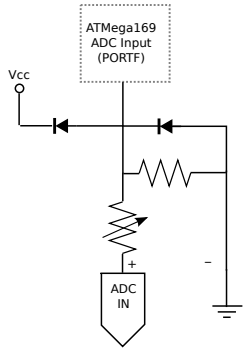

Figure 5: ADC4,6,7 Input

For making voltage measurements above V_{cc}, a voltage divider allows reduction of the voltage at the ADC. By constructing the voltage divider using a variable resistor, the range of measurable inputs could be manually adjusted.

The diodes shown in Figure 5 ensure that the ADC is protected from accidental exposure to voltages outside the acceptable range. In normal operation both diodes are off. If V_{adc} were to become greater than the reference point V_{cc}, current would flow between the ADC input and the reference point, acting to reduce V_{adc} until it reached V_{cc}. Similarly, if V_{adc} fell below ground, current would flow from ground to the ADC input, acting to increase V_{adc} until it reached ground.

The voltage at the ADC input can be related to the input of the voltage divider using Kirchoff's Voltage Law and Ohm's Law:

$$V_{\text{adc}} = \frac{R_1}{R_1 + R_2} V_{\text{in}}$$

Where V_{in} is the voltage at the input of the circuit, R_1 is a fixed resistor, and R_2 is variable resistor.

V_{in} can be therefore be determined from the registered ADC counts by:

$$V_{\text{in}} = \left(\frac{\text{ADC counts}}{2^{10}} \right) \times \frac{R_1 + R_2}{R_1} V_{cc}$$

Differential ADC Input

During the testing of the TCS experimental apparatus, it became desirable to measure the emission current of the electron gun. The electrometer used for this current measurement was capable of producing an analogue

output in the range of $0-1V$. However, the negative terminal of this output was not at ground potential, but rather at the same terminal as the negative input terminal. Directly connecting the electrometer output to one of the ADC inputs discussed above would create a short circuit between the initial energy power supply, and ground (refer to Figures **??** and **??**). Therefore, it was decided to add a differential stage before the input of one of the ADCs.

Figure 6 shows the modification made to the input for ADC5 on the AVR Butterfly. The original voltage divider and input protection discussed above are still present. The modifications include the addition of an instrumentation amplifier, and low pass filters.

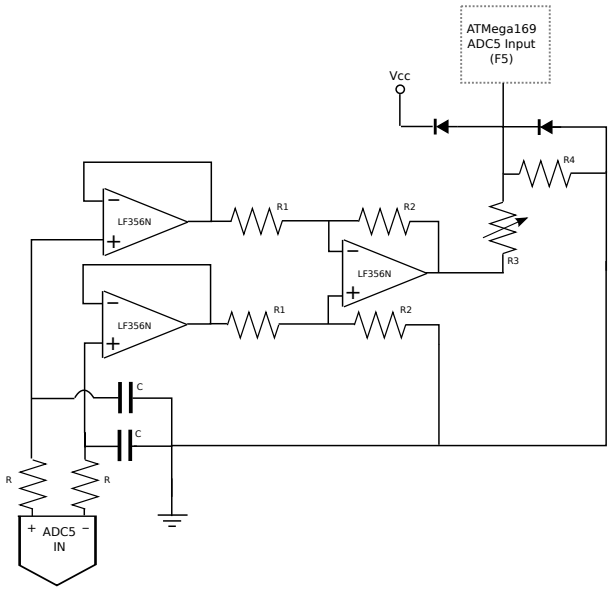

Figure 6: Differential Input stage for ADC5

asdfa The instrumentation amplifier consists of two stages of operational amplifiers (op-amps); input buffers, and a difference amplifier. The difference amplifier can be shown using the ideal op-amp model to produce an output voltage proportional to the difference between its inputs:

$$V_{out} = \frac{R_2}{R_1}(V_2 - V_1)$$

The two op-amps at the inputs to the differential amplifier are unity gain buffers. Although the outputs of the op amps are equal to their inputs, current is prevented from flowing from the circuit under measurement, and is instead drawn from the op amp power supply.

In principle, two ADC channels could be used to record the positive and negative outputs of the electrometer seperately, with differencing done in software. However this would require modification to the output cable of the electrometer, which may prove inconvenient for future uses.It was decided that the modification of the cable and added complexity of the software required would be more time consuming than differencing the two inputs using the hardware methods described above.

The low pass filters were added to the inputs of ADC5 after it was found that an unacceptable level of AC noise was being output by the electrometer. The level of noise was too high to be filtered in software, for reasons that will be discussed in Appendix D.

Temperature Measurement

The AVR Butterfly features an onboard thermistor connected to ADC0. Reading ADC0 and applying the formula given in the AVR Butterfly User's Guide [] results in a temperature measurement. This was useful in establishing a link between the changing chamber pressure and the temperature of the laboratory (see Appendix C).

Power Supplies

Due to the presence of both analogue and digital electronics in the DAC/ADC box, three seperate supply voltages were required:

1. Digital logic in the range $3 \rightarrow 4.5$V
2. Positive op-amp supply in the range $10 \rightarrow 15$V
3. Negative op-amp supply in the range $-10 \rightarrow -15$V

Circuitry was designed which allowed two seperate single pole power supplies to be used for Digital logic and the op-amps. A dual 0-30V DC power supply has been used for both digital and analogue circuitry.

Logic Power Supply

The AVR Butterfly runs off $3V < V_{cc} < 4.5V$ DC. Since V_{cc} was also used as the reference voltage for the ADCs and DAC output, it was desirable that V_{cc} be kept constant, despite the absolute level of the power supply. A $3.3V$ voltage regulator has been used for this purpose. The capacitor further smooths the output by shorting high frequency fluctuations to ground.

When the DAC/ADC box was first constructed V_{cc} was supplied by three $1.5V$ batteries. However, due to higher than expected power usage, and the unreliability of the voltage regulator as the input voltage fell below $4V$, inputs for an external power supply were later added.

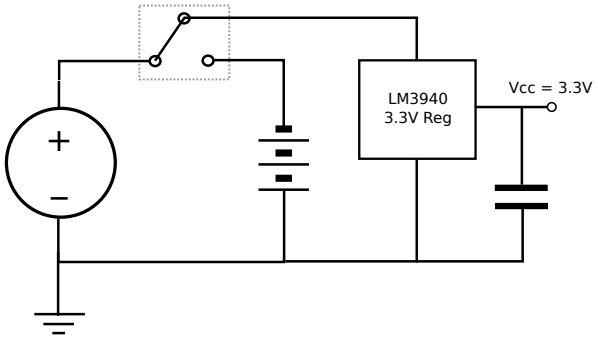

Figure 7: Logic Power Supply

Op-amp Power Supply

The DAC/ADC box circuitry involves several operational amplifiers (LF356), which require dual $\pm 10 - 15V$ supplies. As there were no dual $\pm$ power supplies available, a single $30V$ power supply was used, with the circuit shown in figure **??** used to produce $\pm 15V$ relative to ground.

The buffer amplifier ensures that negligable current can flow from the power supply into the logic and ADC circuits, whilst the capacitor removes high frequency fluctuations of the power supply relative to ground.

DAC Output

A commercial DAC board was used to produce the DAC output. The Microchip MCP4922 ET-Mini DAC is controlled by the AVR Butterfly using Motorola's Serial Peripheral Interface (SPI) Bus. The software used to implement SPI between the MCP4922 and the AVR Butterfly is discussed in Appendix D.

The ET-Mini DAC can only be powered off $3V$ to $5V$. Using $V_{cc} = 3.3V$ means that the DAC output cannot exceed $V_{cc} = 3.3V$. For TCS, energies of up to $15eV$ are required, so amplification of the DAC output was clearly necessary. A simple non-inverting amplifier with a manually adjustable gain was used to amplify the DAC output by a factor of three. This output was then used to control a laboratory power supply to produce the full range of initial energies.

RS-232 Communications

The AVR Butterfly features an onboard USART, which can be used both for programming and communication with the ATMega169 processor. The RS-232 communications requires only three wires; Recieve (RX), Transmit (TX) and a common ground.

The requirement that the AVR Butterfly share a common ground with the controlling computer lead to increased noise through ground loops. This is discussed in more detail in Appendix D.

Although the RS-232 is relatively simple to implement, which makes it ideal for non-proprietry microprocessor applications, most modern computers no longer feature RS-232 COM ports. Although a computer with COM ports was available at CAMSP, due to the extreme unreliability of this computer, it was quickly replaced with a laptop that did not possess COM ports, and a commercial RS-232 to USB converter was used to interface with the laptop.

Appendix C - Pressure Monitoring

The pressure in the chamber was monitored by a ion gauge at low pressure (below 10^{-3} mbar), and a pirani gauge at high pressure. The gauge included a flurescent Liquid Crystal Display (LCD). In order to automate monitoring of pressure, a USB webcam was placed in front of the gauge LCD. Software was written using the Python Imaging Library (PIL) to convert the image produced by the webcam into a pressure reading. In this way, the pressure could be recorded as a function of time, independent from other measurements performed using the ADC/DAC control box.

Figures 8 to 10 show the process by which an image taken with the webcam was converted into a pressure reading. The software first identifies bounding rectangles for each individual digit. These are then further subdivided into 7 segments. If enough pixels in a given segment match the colour LCD segments, then the segment can be identified as activated. The software then creates a string corresponding to the activated segments, and looks up the digit in a dictionary.

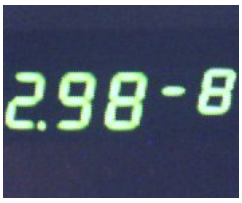

Figure 8: An unprocessed image

Figure 9: Individual digits identified

Figure 10: Activated segments (green) for a single digit

Appendix D - Sources of Error

GROUND LOOOOOOPS!

Appendix E - Software

No really, you don't want to know

References

[1] A. H Pfund. Bismuth black and its applications. *Review of Scientific Instruments*, 1930.

[2] A. H Pfund. The optical properties of metallic and crystalline powders. *Journal of the Optical Society of America*, 1933.

[3] Benjamin M. Siegel Louis Harris, Rosemary T. McGinnies. The preparation and optical properties of gold blacks. *Journal of the Optical Society of America*, 1948.

[4] Louis Harris and John K. Beasley. The infrared properties of gold smoke deposits. *Journal of the Optical Society of America*, 1952.

[5] Louis Harris and Arthur L. Loeb. Conductance and relaxation time of electrons in gold blacks from transmission and reflection measurements in the far infrared. *Journal of the Optical Society of America*, 43(11), 1953.

[6] D. R. McKenzie. Selective nature of gold-black deposits. *Applied Optics*, 2006.

[7] Tobias Holmgaard Thomas Sndergaard, Sergey M. Novikov, Rene L. Eriksen, Jonas Beermann, Zhanghua Han, Kjeld Pederson, and Sergey I. Bozhevolnyi. Plasmonic black gold by adiabatic nanofocusing and adsorption of light in ultra-sharp convex grooves. *Nature Communications*, 2012.